Highly Localized Delivery of Microwaves to Quantum Bits with a Scanning Loop Micro-Antenna

Sangjun Noh[#], Minghao Jiang[$], Javier Noé Ramos-Silva[#], Philip Hemmer[*], Kamel Haddadi[^], Peter J. Burke[#1]

[#]Department of Electrical Engineering and Computer Science, University of California, Irvine, USA
[$]Department of Physics and Astronomy, University of California, Irvine, USA
[*]Department of Electrical and Computer Engineering, Texas A&M University, USA
[^]University of Lille, CNRS, Univ. Polytechnique Hauts-de-France, UMR 8520 - IEMN, France
[1]pburke@uci.edu

***Abstract*— We demonstrate highly localized delivery of microwaves to quantum bits with a scanning loop micro-antenna. The quantum state of the qubits (ensembles of nitrogen vacancy centers in microdiamond) is read out optically, via Optically Detected Magnetic Resonance (ODMR). A 600 × 600 μm^2 via-based PCB loop antenna is used as the excitation source. A piezo micromanipulator from Sensapex™ provides precise control of the antenna position above microdiamond containing nitrogen-vacancy (NV) centers, enabling spatially resolved ODMR measurements. Line- and two-dimensional imaging scans reveal the local microwave near-field distribution generated by the loop antenna. These results demonstrate spatially resolved ODMR mapping using a custom-built free-space optical configuration and establish a basis for future NV-based quantum sensing and microwave field characterization, as well as laying the foundation for quantum state manipulation of individual qubits using programmable, highly localized delivery of microwaves.**

***Keywords*— nitrogen-vacancy (NV) centers, optically detected magnetic resonance (ODMR), scanning ODMR, piezo micromanipulator, microwave near-field mapping, PCB antenna**

I. Introduction

Quantum sensing based on solid-state spins offers a powerful route for precision measurements of electromagnetic fields [1], [2], [3], frequency shifts [3], [4], [5], and thermal variations [6], [7] under ambient conditions. Among available platforms, nitrogen–vacancy (NV) centers in microdiamond provide optical initialization and readout, long spin coherence, and stable performance at room temperature [4], [8]. Unlike conventional near-field probes that may perturb the device under test (DUT), NV centers act as passive spin-based magnetic field sensors, enabling non-contact microwave magnetic field imaging with micron-scale spatial resolution. When excited by a green laser, the NV center relaxes into the $m_s = 0$ spin sublevel of its electronic ground state (where m_s denotes the spin projection quantum number), while a resonant microwave field drives transitions to the $m_s = \pm 1$ sublevels and produces a measurable fluorescence reduction. This spin-dependent fluorescence change enables optically detected magnetic resonance (ODMR), which serves as a key mechanism for NV-based sensing.

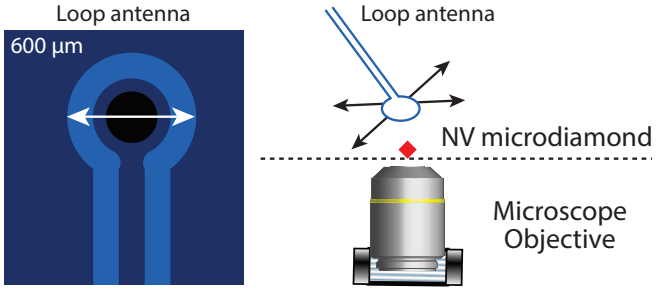

Fig. 1. Conceptual schematic of the scanning geometry. A 600 × 600 μm^2 microwave loop antenna is scanned above an NV-containing microdiamond to measure spatial variations in fluorescence and ODMR contrast.

Spatially resolved ODMR measurements require instrumentation capable of coordinating optical fluorescence detection with position-dependent delivery of microwave excitation. Super-resolution fluorescence techniques can improve the signal-to-noise ratio and optical resolution of NV emission [9], and in our previous work, we demonstrated ODMR feasibility using an off-the-shelf confocal/super-resolution microscope [10]. However, such measurements do not provide the ability to scan a microwave source over the microdiamond or map ODMR contrast as a function of antenna position.

Related scanning microwave microscopy (SMM) based sensing have demonstrated that spatially resolved microwave–to-material interactions can be obtained by mechanically translating a local microwave probe. In our earlier work, we used an interferometric tuned-reflectometer SMM system to measure nanoscale impedance variations in liquid biological samples [11], and in subsequent work, we combined a coaxial three-dimensional scanning microwave probe with super-resolution fluorescence imaging to map position-dependent microwave coupling [12]. These SMM studies show that controlled probe translation enables spatial mapping of microwave interactions, motivating scanning-based sensing methods for quantitative near-field characterization.

Quantitative characterization of local microwave near-fields demands a platform that can directly measure spatial variations in ODMR response. Recent wide-field NV-ensemble work by Basso *et al.* [13] imaged microwave field strength through differential Rabi shifts generated by a device under test (DUT), but the fixed NV layer geometry

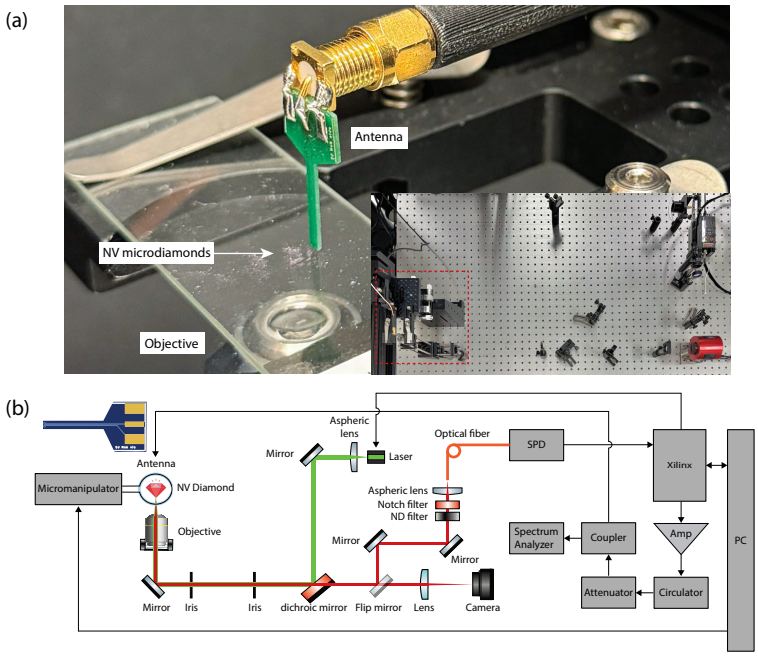

Fig. 2. (a) Zoomed-in view of the vertically mounted loop antenna above the NV microdiamond. The inset shows the full optical setup, with the dashed box marking the antenna–microdiamond region. (b) Schematic of the scanning ODMR system. The Xilinx™ RFSoC 4x2 development board (four RF ADCs and two RF DACs) generates microwave signals and acquires single photon detector (SPD) data, while a Python-controlled PC manages the overall operation. A via-based 600 × 600 μm^2 loop PCB antenna mounted on a micromanipulator is scanned above the NV microdiamond, and NV fluorescence is collected through the optical path for ODMR measurements.

prevented true position-dependent scanning of the microwave source.

In this work, we present a scanning ODMR platform that integrates a custom-built free-space optical system, a via-based PCB loop antenna, and a precision piezo micromanipulator. By translating the loop antenna across the microdiamond surface and recording the corresponding fluorescence and ODMR contrast, the system directly visualizes the microwave near-field produced by the loop. Unlike static ODMR or wide-field imaging, this approach resolves how ODMR contrast changes with antenna position, enabling spatially dependent microwave field measurements.

The conceptual geometry of the scanning configuration is shown in Fig. 1. A 600 × 600 μm^2 microwave loop antenna is positioned approximately 150 μm above an NV-containing microdiamond and scanned in the x–y–z directions to measure position-dependent fluorescence and ODMR contrast.

II. Experimental Set-up

Fig. 2 shows the configuration of the scanning ODMR system. The platform consists of a free-space optical path, a via-based PCB loop antenna with dimensions of 600 × 600 μm^2, an RFSoC-based control/data-acquisition board (Xilinx™ RFSoC 4×2 board), a high-power microwave amplifier (Mini-Circuits™ ZHL-16W-43-S+), a variable attenuator (Narda™ Microline 4704-99), a directional coupler (MAC Technology Inc.™, 20 dB), a spectrum analyzer (RIGOL™ DSA832E), and a three-axis piezoelectric micromanipulator (Sensapex™ μMp-3). The RFSoC board generates microwave signals and digitizes fluorescence data, while all components are synchronized through a Python control program running on a PC.

The antenna geometry orients the loop perpendicular to the front face of the PCB, allowing it to be positioned vertically relative to the NV microdiamond drop-cast on a microscope slide. This vertical placement reduces parasitic coupling to the ground plane or other conductors, improving stability during near-field measurements. The antenna was mounted on the Sensapex™ stage and positioned approximately 150 μm above the microdiamond, enabling precise three-dimensional scanning during ODMR acquisition.

The NV microdiamond was prepared by drop-casting microdiamonds with an average diameter of ∼15 μm onto a glass slide. Because each microdiamond exhibits a distinct crystallographic orientation, their ODMR resonance frequencies may differ slightly under identical experimental conditions [14]. Therefore, the resonance frequency of the selected microdiamond was measured prior to scanning.

ODMR measurements were performed by detecting NV fluorescence using a single-photon detector (SPD). The Xilinx™ RFSoC 4×2 swept the microwave frequency from 2.7 to 3.0 GHz (+35 dBm) in 1 MHz increments while recording fluorescence counts. The resulting spectra were fitted with Lorentzian functions to determine the resonance frequency and the optimal microwave power. For scanning ODMR measurements, the microwave frequency was fixed at the determined resonance (2874 MHz), and the loop antenna was translated above the microdiamond while fluorescence time

traces were recorded. All data were processed and visualized using Igor Pro 9 (WaveMetrics data analysis software).

III. Experimental Results

Fig. 3 summarizes the initial ODMR characterization of a single NV microdiamond. As shown in Fig. 3(a), photoluminescence (PL) imaging (with the microwave source turned off) was first used to locate and select an individual microdiamond prior to ODMR measurements. ODMR was measured in a continuous-wave (CW) configuration while monitoring NV fluorescence, with each frequency point averaged 500 times to suppress noise.

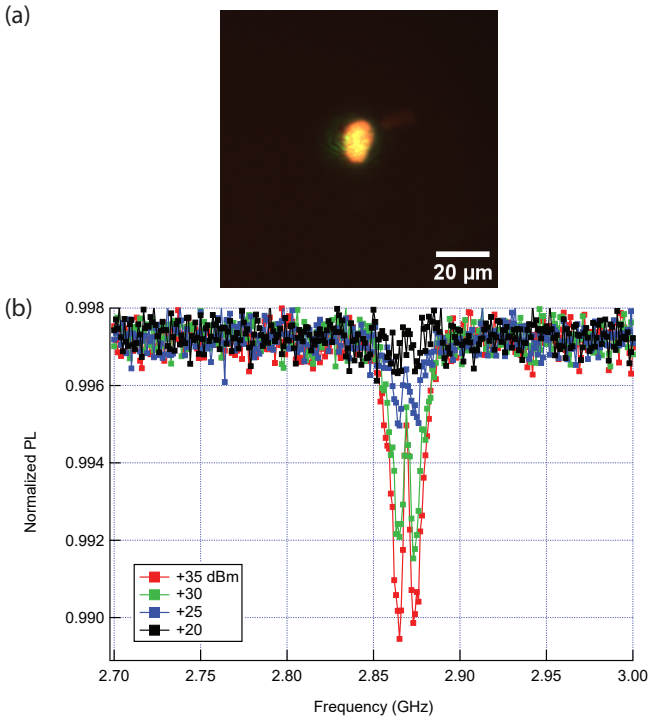

Fig. 3. (a) PL image of a selected NV microdiamond. (b) ODMR spectra measured at different microwave powers (+20, +25, +30, +35 dBm), showing a resonance near 2874 MHz.

The microwave frequency was swept from 2.7 to 3.0 GHz in 1 MHz steps, and Fig. 3(b) compares the spectra obtained at four microwave power levels (+20, +25, +30, and +35 dBm). A clear resonance dip appears near 2874 MHz under all conditions. At +35 dBm, the contrast reached approximately 1%, and the full-width at half-maximum (FWHM) was measured to be 2.1×10^7 Hz, corresponding to a contrast–linewidth ratio of 4.76×10^{-10} Hz^{-1}. Because crystallographic orientation differences can shift the resonance frequency between microdiamonds [14], this microdiamond-specific resonance (2874 MHz at +35 dBm) was used in subsequent scanning measurements.

Fig. 4 presents the one-dimensional scanning ODMR results obtained by translating the loop antenna across the selected NV microdiamond. The PL intensity profile (blue curve) and ODMR contrast profile (red curve) both exhibit a pronounced dip at the microdiamond location,

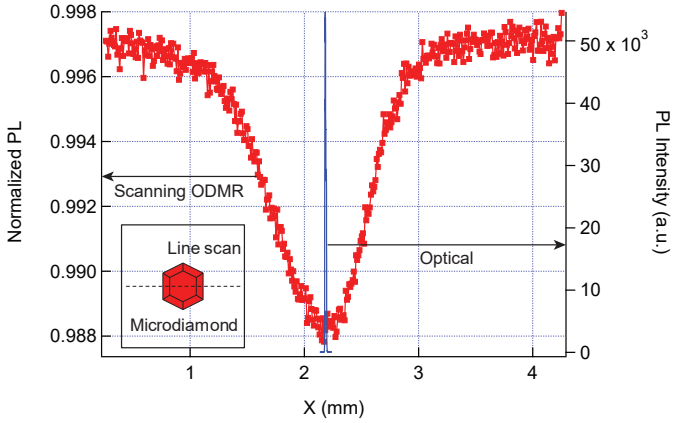

Fig. 4. One-dimensional line profiles of fluorescence intensity (blue) and scanning ODMR contrast (red) across a single NV microdiamond. Both traces display a co-localized dip at the microdiamond position, confirming precise spatial alignment between fluorescence imaging and ODMR scanning

demonstrating spatial correspondence between optical imaging and microwave-driven resonance changes. The PL profile exhibited a FWHM of approximately 16 μm, similar to the physical size of the microdiamond, whereas the ODMR response extended over $\sim$970 μm. This broad spatial response arises from the near-field distribution generated by the 600 $\times$ 600 μm^2 loop antenna positioned 150 μm above the microdiamond.

Fig. 5 shows the two-dimensional scanning ODMR map. The antenna was scanned across a 4 $\times$ 4 mm^2 region in the X–Y plane with 100 μm step size, and NV fluorescence was recorded at each position. A strong PL reduction appeared near the center of the scan region, where the microwave near-field was strongest, and the fluorescence gradually recovered toward the outer region. This map visualizes the spatial footprint of the microwave near-field generated by the via-loop antenna and is consistent with the wide profile observed in the line-scan measurements.

IV. Discussion

The scanning ODMR measurements performed with the PCB-based loop antenna demonstrate that the position of an NV microdiamond can be spatially identified through comparison with the optical fluorescence profile. As shown in Fig. 4, both traces exhibit a co-localized dip, confirming alignment between optical imaging and ODMR detection.

A substantial difference in spatial width, however, was observed between the two signals. The optical fluorescence profile shows an FWHM of about 16 μm, whereas the ODMR response extends to roughly 970 μm. This broadening arises from the 600 $\times$ 600 μm^2 PCB loop, selected as a proof-of-concept design constrained by fabrication limits, which expands the microwave near-field at 150 μm spacing.

The two-dimensional scan in Fig. 5 shows the same trend, with maximum PL reduction near the scan center and gradual recovery outward. These results demonstrate that the platform provides a spatial map of the microwave near-field

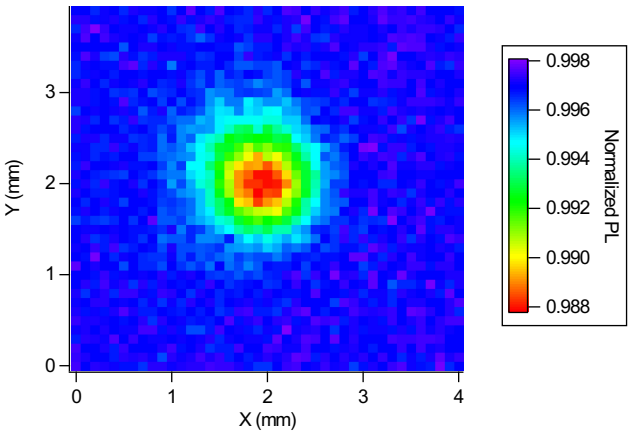

Fig. 5. Two-dimensional scanning ODMR map. The antenna was scanned over a 4 × 4 mm^2 area with a 100 μm step interval while recording NV fluorescence. A strong PL reduction appears near the center, corresponding to the maximum microwave near-field strength, and the ODMR effect gradually weakens toward the outer region.

distribution, while antenna geometry dominates the apparent spatial footprint. Compared to wide-field ensemble methods such as Basso *et al.* [13], which infer microwave variations from differential Rabi shifts, our scanning ODMR approach directly measures contrast changes as the loop antenna is repositioned, so the observed footprint reflects the antenna's near-field rather than DUT-generated fields.

V. Conclusion

We developed a scanning ODMR platform that integrates a custom-built optical system with a PCB-based loop antenna, enabling spatial mapping of ODMR contrast around NV microdiamonds. ODMR spectroscopy identified the resonance frequency and microwave power, and subsequent line- and area-scans visualized the microwave near-field in one and two dimensions.

The coincidence of fluorescence and ODMR dips confirms accurate NV localization. The much broader ODMR width (~970 μm) compared to the optical FWHM (16 μm) indicates that spatial resolution is primarily limited by the loop-antenna size and its field distribution. Smaller microwave sources are expected to confine the field below the 15 µm microdiamond size used here, and ongoing development of micron-scale coaxial loop antennas aims to further localize microwave delivery for future single-NV studies.

Overall, the platform establishes a compact and practical method for NV-based microwave field mapping and offers a basis for future high-resolution quantum sensing. We envision the next generation of this platform to allow localized delivery of microwave pulse sequences to individual quantum bits, enabling quantum state manipulation, for a scalable, programmable quantum bit addressing scheme for applications in quantum information science and technology.

References

[1] G. Balasubramanian, I. Y. Chan, R. Kolesov, M. Al-Hmoud, J. Tisler, C. Shin, C. Kim, A. Wojcik, P. R. Hemmer, A. Krueger, T. Hanke, A. Leitenstorfer, R. Bratschitsch, F. Jelezko, and J. Wrachtrup, "Nanoscale imaging magnetometry with diamond spins under ambient conditions," *Nature 2008 455:7213*, vol. 455, pp. 648–651, 10 2008.

[2] J. F. Barry, J. M. Schloss, E. Bauch, M. J. Turner, C. A. Hart, L. M. Pham, and R. L. Walsworth, "Sensitivity optimization for nv-diamond magnetometry," *Reviews of Modern Physics*, vol. 92, p. 015004, 3 2020.

[3] F. Dolde, H. Fedder, M. W. Doherty, T. Nöbauer, F. Rempp, G. Balasubramanian, T. Wolf, F. Reinhard, L. C. Hollenberg, F. Jelezko, and J. Wrachtrup, "Electric-field sensing using single diamond spins," *Nature Physics 2011 7:6*, vol. 7, pp. 459–463, 4 2011.

[4] J. M. Taylor, P. Cappellaro, L. Childress, L. Jiang, D. Budker, P. R. Hemmer, A. Yacoby, R. Walsworth, and M. D. Lukin, "High-sensitivity diamond magnetometer with nanoscale resolution," *Nature Physics*, vol. 4, pp. 810–816, 9 2008.

[5] C. L. Degen, F. Reinhard, and P. Cappellaro, "Quantum sensing," *Reviews of Modern Physics*, vol. 89, p. 035002, 7 2017.

[6] G. Kucsko, P. C. Maurer, N. Y. Yao, M. Kubo, H. J. Noh, P. K. Lo, H. Park, and M. D. Lukin, "Nanometre-scale thermometry in a living cell," *Nature 2013 500:7460*, vol. 500, pp. 54–58, 7 2013.

[7] D. M. Toyli, C. F. D. L. Casas, D. J. Christle, V. V. Dobrovitski, and D. D. Awschalom, "Fluorescence thermometry enhanced by the quantum coherence of single spins in diamond," *Proceedings of the National Academy of Sciences of the United States of America*, vol. 110, pp. 8417–8421, 5 2013.

[8] R. Schirhagl, K. Chang, M. Loretz, and C. L. Degen, "Nitrogen-vacancy centers in diamond: Nanoscale sensors for physics and biology," *Annual Review of Physical Chemistry*, vol. 65, pp. 83–105, 2014.

[9] J. Huff, "The airyscan detector from zeiss: confocal imaging with improved signal-to-noise ratio and super-resolution," *Nature Methods*, vol. 12, p. ii, 12 2015.

[10] S. Noh, M. Jiang, J. J. Leon, P. J. Hemmer, and P. J. Burke, "Quantum sensing with an off-the-shelf super resolution microscope." SPIE-Intl Soc Optical Eng, 3 2025, p. 33.

[11] J. Li, Z. Nernati, K. Haddadi, D. C. Wallace, and P. J. Burke, "Scanning microwave microscopy of vital mitochondria in respiration buffer," *IEEE MTT-S International Microwave Symposium Digest*, vol. 2018-June, pp. 115–118, 8 2018.

[12] C. H. Lee, K. Haddadi, and P. J. Burke, "Combined super-resolution fluorescence and coaxial 3-d scanning microwave microscopy: Proof-of-concept in-liquid live-cell imaging: Toward a biological nano-radar," *IEEE Microwave and Wireless Technology Letters*, vol. 35, pp. 131–134, 2025.

[13] L. Basso, P. Kehayias, J. Henshaw, G. Joshi, M. P. Lilly, M. B. Jordan, and A. M. Mounce, "Wide-field microwave magnetic field imaging with nitrogen-vacancy centers in diamond," *Journal of Applied Physics*, vol. 137, 3 2025.

[14] S. Sengottuvel, M. Mrózek, M. Sawczak, M. J. Głowacki, M. Ficek, W. Gawlik, and A. M. Wojciechowski, "Wide-field magnetometry using nitrogen-vacancy color centers with randomly oriented micro-diamonds," *Scientific Reports*, vol. 12, pp. 1–9, 12 2022.